Natural chromatin is heterogeneous and self associates *in vitro*

Shujun Cai, Yajiao Song, Chen Chen, Jian Shi and Lu Gan*

Department of Biological Sciences and Centre for BioImaging Sciences, National University of Singapore, Singapore 117543

* Correspondence: lu@anaphase.org

ABSTRACT

The 30-nm fiber is commonly found in oligonucleosome arrays *in vitro* but rarely found in chromatin within nuclei. To determine how chromatin high-order structure is controlled, we used cryo-ET to study the undigested natural chromatin released from cells that do not have evidence of 30-nm fibers *in vivo*: picoplankton and yeast. In the presence of divalent cations, most of the chromatin from both organisms is compacted into a large mass. Rare irregular 30-nm fibers do form at the periphery of this mass, some of which include face-to-face interactions. In the absence of divalent cations, picoplankton chromatin decondenses into open zigzags. By contrast, yeast chromatin mostly remains compact with looser nucleosome packing, even after treatment with histone-deacetylase inhibitor. The 3-D configuration of natural chromatin is therefore sensitive to the local environment, but generally nonpermissive of regular motifs, even at the level of oligonucleosomes.

INTRODUCTION

In eukaryotic cells, chromatin is important in nuclear processes like transcription and replication. Chromatin structure is dictated by the 3-D relationship between nucleosomes (~ 146 bp of DNA wrapped around 8 histones). Chromatin can adopt open or compact higher-order structures, influenced by factors like histone post-translational modifications and interactions with chromatin "architectural" proteins (Jenuwein and Allis, 2001; McBryant et al., 2006). Chromatin higher-order structure in turn controls the accessibility to the DNA for both transcription and replication (Collins et al., 2002; Tse et al., 1998).

Chromatin structure has been studied extensively at nucleosome level. Nucleosomes connected by linker DNA are described as "beads-on-a-string" (Olins and Olins, 1974). The beads-on-a-string is hypothesized to be compacted into a helical nucleosome arrangement called the "30-nm fiber", which is proposed to be either a one-start helix or two-start zigzag (Finch and Klug, 1976; Woodcock et al., 1984). However, more than one form of nucleosome packing might also coexist in the same 30-nm fiber (Grigoryev et al., 2009).

The diversity of chromatin structures has lead to inconsistent terminology. For the sake of clarity, we define a chromatin "mass" as a compact body with irregularly packed chromatin; a "regular 30-nm fiber" as an ordered compact structure approximately 30-nm wide; an "irregular 30-nm fiber" as a fiber-like structure with few repeated nucleosome motifs and of variable width; an "open zigzag" as a more extended structure with resolvable linker DNA and few nucleosome-nucleosome

interactions; and the beads-on-a-string as a chain of nucleosomes in which the angle between the entering and exiting linker DNA is nearly 180° (Fig. 1A).

Most of our knowledge of chromatin structure comes from studies of dilute solutions of short nucleosomes chains. These studies have systematically tested the effects of fixation with glutaraldehyde (Athey et al., 1990), recombinant histones (Luger et al., 1997b), linker histones (Routh et al., 2008), artificially selected "Widom 601" sequences that have a high affinity for histones (Dorigo et al., 2004), and ionic conditions (Dorigo et al., 2003; Huynh et al., 2005). Under special conditions, such chromatin constructs can form highly regular 30-nm fibers that can be studied at high resolution (Song et al., 2014).

Chromatin structure has also been studied *in situ* in a life-like frozen-hydrated state, either in 2-D by cryo-EM projection imaging or in 3-D by electron cryotomography (cryo-ET). These studies are much rarer because it is challenging to thin and then image the cells at cryogenic temperatures. Three groups found no evidence of regular 30-nm fibers in mammalian cells (McDowall et al., 1986; Eltsov et al., 2008; Eltsov et al., 2014). We found that in the single-celled organisms *Ostreococcus tauri* (a eukaryotic picoplankton; herein called picoplankton) and *Saccharomyces cerevisiae* (a budding yeast; herein called yeast), there was also no evidence of regular 30-nm fibers (Gan et al., 2013; Chen et al., 2016). In contrast, cryo-EM studies have detected regular 30-nm fibers in the isolated nuclei of both starfish sperm (Woodcock, 1994) and chicken erythrocytes (Scheffer et al., 2011). These and other studies challenge whether 30-nm fibers is the best model of chromatin within somatic cells (Hansen, 2012; Nishino et al., 2012; van Holde and Zlatanova, 1995).

74 The different conclusions between *in vitro* and *in vivo* chromatin studies raise the
75 question: can the chromatin of cells that do not show evidence of 30-nm fibers *in vivo*
76 be made to adopt a 30-nm-fiber structure *in vitro*? To address this question, we used
77 cryo-ET to study the 3-D organization of undigested natural chromatin from
78 picoplankton and yeast. In the presence of even traces of divalent cations, most of the
79 chromatin in both organisms compacts into large masses. Some of the chromatin does
80 form 30-nm fibers, predominantly of the irregular variety. In the absence of divalent
81 cations, picoplankton chromatin decondenses into open zigzags, but yeast chromatin
82 remains either in a mass or folded as irregular 30-nm fibers. To better understand how
83 these nucleosomes interact, we classified the chromatin in both 2-D and 3-D, and found
84 that there is no dominant higher-order packing motif, but the orientation of the DNA at
85 the core-particle entry/exit points is not too variable. Therefore, the higher-order
86 structure of natural chromatin is sensitive to environmental conditions, but this
87 sensitivity varies by species.

RESULTS

Release of natural picoplankton chromatin

To study the higher-order structure of natural picoplankton chromatin *in vitro*, we lysed cells in hypotonic buffer on ice either with or without divalent cations (Fig. 1B). This treatment released all cellular contents, including the chromatin, and is expected to produce thinner plunge-frozen samples that generate higher-contrast cryotomograms. Compared to intact cells (Fig. 1C), the lysed cells' contents spread over a much larger area and indeed allowed the ice to be thinner, resulting in higher-contrast tomograms (Fig. 1D). The majority of the densities came from remnants of the two largest organelles -- the nucleus and the chloroplast. To keep the chromatin as intact as possible, we did not perform any isolation procedures or nuclease digestion.

Picoplankton chromatin forms masses and irregular 30-nm fibers only in the presence of divalent cations

Previous studies have shown that short nucleosome arrays are sensitive to divalent cation concentration (Bednar et al., 1998). To test if divalent cations can induce 30-nm-fibers in undigested picoplankton chromatin, we lysed and imaged picoplankton in the presence of 1 mM Mg^{2+}. Most of the chromatin in these conditions was compacted into a large thick mass, but a small portion of the chromatin did form irregular 30-nm fibers (Figs. 2A and S1). The contrast was too low, however, to reveal more details. To determine how much the compaction and 30-nm fibers depended on Mg^{2+}, we lysed cells without additional divalent cations (Fig. 2B). Under this condition,

most of the chromatin still remained associated as a large compact mass, but with more short irregular 30-nm fibers visible (Figs. 2E,F and S2). As a consequence of the ice thickness and dense nucleosome packing, the contrast was still too low to permit the unambiguous visualization of individual nucleosomes in most tomograms. In rare examples, we found some small clusters of nucleosomes packed in regular face-to-face interactions (Figs. S2G-J).

To determine if picoplankton chromatin masses and irregular 30-nm fibers depend on divalent cations, we chelated the residual divalent cations by lysing cells in the presence of 5 mM Ethylenediaminetetraacetic Acid (EDTA) (Fig. 2C, S3). The EDTA treatment was effective because ribosomes, which require magnesium for stability, were absent (Chao, 1957). In picoplankton samples treated this way, we did not find any evidence of 30-nm fibers or chromatin masses. Instead, all of the chromatin was decondensed into an open zigzag-like motif with individual nucleosomes and naked DNA visible (Fig. 2G). This large-scale change of chromatin higher-order structure demonstrates that picoplankton chromatin higher-order structure is very sensitive to divalent cation concentration.

Yeast chromatin packing is less sensitive to divalent cations than picoplankton

Picoplankton and yeast chromatin do not show evidence of 30-nm fibers *in vivo* (Gan et al., 2013; Chen et al., 2016). To test whether the chromatin higher-order structure of these two organisms is conserved *in vitro*, we imaged yeast chromatin in cell lysate. Yeast chromatin was more difficult to locate in these samples because there was no chromatin-proximal high-contrast structure like the chloroplast. To overcome this

problem, we first isolated and then lysed the nuclei in hypotonic buffer without additional divalent cations (Fig. S4). This strategy made it straightforward to locate the chromatin because it was now the most abundant material on the grid.

Like in picoplankton, the majority of yeast chromatin was compacted in a thick mass (Figs. 3A). This chromatin mass had low contrast, which prevented us from visualizing individual nucleosomes. In rare cases, we saw 30-nm fibers at the periphery of the chromatin mass (Fig. 3A). In total, we observed only seven irregular 30-nm fibers in eleven tomograms. These observations show that in the presence of trace amounts of free magnesium, yeast chromatin compacts *in vitro* and can occasionally form irregular 30-nm fibers.

To test if the yeast chromatin organization depends on residual divalent cations, we lysed nuclei in the presence of EDTA. In the 5 mM EDTA-treated sample, we were unable to distinguish most nucleosomes because the chromatin was not dispersed enough (Fig. S5A,C,D). Intact ribosomes could still be found, indicating that trace amounts of divalent cations were still present (Fig. S5A and C). We therefore increased the lysis-buffer EDTA concentration to 50 mM. This new condition was more effective because we could not find any 80S ribosomes (Fig. S5B and E). In the presence of 50 mM EDTA, the chromatin mass became more dispersed (Fig. S6), and unlike in the conditions with less EDTA, chromatin fibers thicker than 50 nm were no longer detectable (Fig. S6). Unlike in picoplankton, in the absence of divalent cations, yeast nucleosomes remained closely packed and were not found to adopt the open zigzags with visible linker DNA (Fig. 3B, more examples in Fig. S5E and F). In summary, natural

yeast chromatin can compact into a large mass and form irregular 30-nm fibers even in the absence of divalent cations.

Histone deacetylation facilitates yeast chromatin compaction

In an early study (Lowary and Widom, 1989), yeast chromatin fragments in low salt formed extended “10-nm filaments”. We did not observe such structures. While the conditions in that study were different from ours (traditional EM vs. cryo-EM; digested vs. undigested chromatin), we sought another explanation for the differences observed. It is known that yeast chromatin is susceptible to deacetylation when cells are disrupted (Waterborg, 2000). To test whether the histone acetylation levels in yeast chromatin *in vitro* were too low to support a more disperse structure like the open zigzag, we treated the intact cells with Trichostatin A (TSA), a histone-deacetylase inhibitor (Bernstein et al., 2000). We then lysed the cells in hypotonic buffer containing both EDTA and TSA. We found that chromatin isolated this way was indeed more disperse (Figs. 4A and B, more examples in Fig. S7). In rare cases, we found open-zigzags (Figs. 4C and D), but we still did not find any structures that resembled a 10-nm filament. These results are nevertheless consistent with a recent study that showed that histone acetylation makes chromatin more deformable (Shimamoto et al., 2017).

To analyze the nucleosome packing more quantitatively, we performed template matching and then analysed both the nearest-neighboring distance (NND) and 10^{th} NND distributions. The NND reports on short-range compaction whereas the 10^{th} NND reports on long-range compaction, e.g., inter-fiber interactions (Fig. S8). As a reference, we also performed this analysis for nucleosome-like densities *in vivo* (Chen et al.,

2016). The NND distribution plots of chromatin *in vivo* and both with and without TSA treatment were almost indistinguishable (Fig. 4H). Note, however, that template matching *in vivo* produces more false positives due to lower contrast and the presence of more non-nucleosomal macromolecular complexes. These extra false positives make the *in vivo* NND values lower than they really are. Therefore, nucleosomes are very likely to be packed more loosely *in vivo*. In contrast, the 10th NND distribution of TSA-treated chromatin was longer than chromatin *in vivo*, which was itself longer than untreated chromatin *in vitro* (Fig. 4I). Our NND analysis is consistent with chromatin's appearance: histone acetylation does not severely perturb short-range interactions, but does affect long-range interactions between groups of nucleosomes.

In the chromatin of TSA-treated yeast, we observed a few stretches of naked DNA between nucleosomes (Fig. 4B,E,F). Nucleosome-free regions are a form of non-nucleosome-associated DNA that are usually longer than one nucleosome's worth of DNA (Lee et al., 2007; Mavrich et al., 2008; Shivaswamy et al., 2008; Yuan et al., 2005). To test if the long stretches of naked DNA could be nucleosome-free regions, we measured their lengths. We found that most of the naked DNA is between 50 nm and 100 nm long, which is compatible with the absence of one or two nucleosome core particles (each 50 nm long) (Fig. 4G). Our data would also be consistent with the notion that this naked DNA was wrapped around a 'fragile' nucleosome or pre-nucleosome *in vivo*, but then lost their histones during nuclear lysis (Fei et al., 2015; Kubik et al., 2015). On some of the naked DNA strands, we found densities that are smaller than a nucleosome (Fig. 4E). We speculate that these densities might be chromatin-associating protein complexes such as transcription factors, chromatin remodelers, or

their subunits or subnucleosomal particles. Taken together, our *in vitro* DNA-length measurements are consistent with nucleosome-mapping studies.

Natural chromatin has few ordered positions

The crystal structure of a tetranucleosome and the cryo-EM structures of 30-nm fibers both have zigzag motifs with face-to-face nucleosome packing (Schalch et al., 2005; Song et al., 2014). In yeast chromatin, we found that only a few nucleosomes were packed face-to-face (Fig. 5A) or in a zigzag motif (Fig. 5B). To detect more regular packing motifs, we performed 2-D classification on subtomograms that contained multiple nucleosomes (Fig. 5C). In agreement with our visual inspection, only one class showed face-to-face packing and furthermore, there was no dominant motif (Fig. 5C).

Artificial nucleosome arrays with a 167-bp repeat (identical to the yeast nucleosome repeat length) are organized as compact 30-nm fibers (Routh et al., 2008). To test if natural yeast chromatin fibers (Fig. 5D) are as compact as these artificial 30-nm fibers, we determined the number of nucleosomes per 11 nm in the best-resolved fibers (Fig. 5E). Compared to the artificial fibers, most natural fibers are less compact (~1.5 vs 6.1 nucleosomes per 11 nm) and have a broader distribution of diameters (15 to 45 nm vs. 15 to 25nm, Fig. 5E) (Routh et al., 2008). The two best-resolved picoplankton 30-nm fibers (Fig. S2G and H) were also loosely packed (3.3 and 2.4 nucleosomes / 11 nm). Therefore, natural chromatin fibers are less compact but much more heterogeneous than artificial fibers.

Natural chromatin is not very heterogeneous at the nucleosome level

The complexity of natural chromatin could be explained if the nucleosomes are themselves conformationally heterogeneous. To test this hypothesis, we developed a subtomogram analysis workflow that takes advantage of recent advances in 2-D and 3-D image classification (Figs. 6, 7, S9) (Bharat and Scheres, 2016). This approach was able to resolve a few nucleosome conformers that differ in linker DNA orientation. For picoplankton, linker DNA conformation was variable, but the conformers generally fell into three classes (Figs. 6A, S10). In two classes, the linker DNA strands frequently entered and exited the nucleosome core in an “open” instead of “crossed” conformation (Fig. 6A, black and red arrows, respectively; Movie S1). In the third class, only one linker DNA was consistently in the same orientation, and therefore visible. While the 3-D classification in yeast nucleosomes showed higher-resolution features like the DNA gyres of nucleosomes, the linker DNA could not be visualized in most classes except for one class showing a DNA stem-like structure, which might be associated with linker histones (Fig. 7A). Taken together, our 3-D classification reveals that the conformation of nucleosomes is not very heterogeneous, except in the linker DNA.

Even though some of our tomograms reveal the locations of individual nucleosomes, the tomograms are still so crowded and complex that we may have missed some higher-order structures by visual inspection. To further test if the nucleosomes pack into higher-order structures, we remapped the class averages of template-matched nucleosomes into a phantom volume the same size of the original tomogram to make a “synthetic tomogram”. This approach is similar to the work done on polysomes and purified oligonucleosomes (Brandt et al., 2009; Scheffer et al., 2012). Most of the nucleosomes of open zigzags and an example chromatin fiber were

248 visualized in the synthetic tomograms, showing the robustness of our approach (Fig. 6B
249 and C and 7B and C). In both picoplankton and yeast, the nucleosomes do not form
250 long repeating motifs or regular structures of any kind (Fig. 6C and 7E). Furthermore,
251 there were no nucleosome clusters or chains formed by the same conformational class.
252 Therefore, natural chromatin is structurally heterogeneous at the oligonucleosome level.

DISCUSSION

Our previous cryo-ET studies of picoplankton and yeast challenged the notion that the 30-nm fiber explained most chromatin *in vivo* in unicellular eukaryotes. Here, we have tested how natural chromatin is organized *in vitro*, but using undigested natural chromatin instead of the chromatin fragments found in most *in vitro* studies. This natural chromatin condenses as fibers and masses at much lower divalent-cation concentrations than needed for chromatin fragments (Hansen, 2002; Maeshima et al., 2016). In the absence of divalent cations, picoplankton chromatin decondenses to an open zigzag configuration but yeast chromatin retains an irregular 30-nm fiber configuration. This discrepancy is highlighted in yeast chromatin, which, as discussed below, did not unfold as expected. These observations reveal that natural chromatin is both plastic and unpredictable.

Picoplankton and yeast chromatin have different sensitivity to divalent cations

Sequestration of divalent cations with EDTA is known to disrupt 30-nm-fiber formation and oligomerization (Widom, 1986). We found that the chromatin of both picoplankton and yeast is more disperse in the absence of divalent cations, but the level of dispersion is different. Picoplankton chromatin adopts an open zigzag configuration whereas the yeast chromatin is much more crowded, with a few irregular 30-nm fibers, even in 50 mM EDTA (Fig. 8). According to an early study (Lowary and Widom, 1989), the yeast chromatin should have become 10-nm filaments. We did not observe such structures, probably due to the sample differences, e.g., purified short yeast chromatin fragments vs. nuclear lysate. Natural picoplankton chromatin therefore follows the

276 divalent-cation-dependent compaction behavior seen in metazoans, whereas yeast
277 chromatin does not.

278 What factors could explain the differences in the higher-order structure of
279 picoplankton and yeast chromatin? First, the nucleosome-repeat length of picoplankton
280 is ~ 30 bp longer than yeast (Thomas and Furber, 1976; Gan et al., 2013). The shorter
281 yeast linker DNA brings nucleosomes closer together, increasing the chances of
282 interaction between sequential nucleosomes. Second, picoplankton does not have a
283 linker-histone homolog, but yeast does (Downs et al., 2003). Linker histones could keep
284 yeast chromatin compact by, for example, restricting the angles between entering and
285 exiting DNA, which would further disfavor an open zigzag conformation (Thoma and
286 Koller, 1977; Bednar et al., 1998). Third, picoplankton linker DNA is enriched in
287 methylation (Huff and Zilberman, 2014), which stiffens DNA (Nathan and Crothers,
288 2002). This stiffer linker DNA may keep picoplankton nucleosomes apart as open
289 zigzags in the absence of divalent cations. We hypothesize that linker DNA length and
290 chemistry and the presence of linker histone jointly contribute to chromatin
291 compactability.

292

293 **Nucleosomes of natural chromatin pack heterogeneously**

294 Linker DNA has variable length and enters and leaves the nucleosome core
295 particle at variable angles (Yao et al., 1990; Bednar et al., 2017). In the context of
296 undigested chromatin, we also detected linker DNA of differing orientations in the 3-D
297 classes of picoplankton nucleosomes (Fig. 6A). Unlike the cryo-EM study on
298 reconstituted nucleosome arrays (without linker histone) where most nucleosomes had

299 linker DNA in the “closed” conformation (Geiss et al., 2014), we find that picoplankton
300 linker DNA adopts a more “open” conformation, possibly due to the enhanced stiffness
301 of picoplankton linker DNA (see above). In contrast, most 3-D classes of yeast
302 nucleosomes did not show linker DNA, probably due to the crowded packing of
303 nucleosomes that lowers its contrast. We nevertheless saw a stem-like density in one
304 class, similar to a recently published structure of the chromatosome (Bednar et al.,
305 2017).

306 Beads-on-a-string motifs are characterized by the large ~ 180° angle made by
307 the linker DNA at the nucleosome entry and exit points (Fig. 1A, structure v). Repetition
308 of this motif maximizes the distance between nucleosomes, resulting in maximum
309 decondensation. These motifs have been routinely seen in dried chromatin that has
310 been adhered to a carbon film (Olins and Olins, 1974; Grigoryev et al., 2009), but very
311 rarely seen in frozen-hydrated chromatin (Bednar et al., 1998; Geiss et al., 2014). We
312 very rarely saw beads-on-a-string in our picoplankton chromatin and did not see a
313 single example in our yeast chromatin; we surmise that if yeast chromatin adapted the
314 beads-on-a-string configuration, we would have observed a structure that could be
315 called a 10-nm filament. These observations are consistent with the crystal structure of
316 the mononucleosome (Luger et al., 1997), from which the linker DNA would emerge at
317 an angle much less than 180° in the absence of large bending forces. Therefore, the
318 most decondensed conformation that natural chromatin can adopt *in vitro* is an open
319 zigzag.

320 Face-to-face nucleosome packing has been observed in oligonucleosome arrays
321 (Robinson et al., 2006) and isolated starfish sperm chromatin (Scheffer et al., 2012).

Here we found that the face-to-face interactions exist in both picoplankton and yeast, but are rare. The face-to-face packing probably involves the well-known interaction between a positively charged histone tail on one nucleosome with the acidic patch on a neighbor (Luger et al., 1997a; Funke et al., 2016). The rarity of face-to-face packing in natural chromatin is at odds with the cryo-EM models of recombinant 30-nm fibers, in which every single nucleosome is involved in a face-to-face packing interaction (Song et al., 2014). In that study, the absence of histone marks, the glutaraldehyde fixation, and the periodic spacing between adjacent nucleosomes could have stabilized the face-to-face packing interaction, thereby explaining why the structures of reconstituted nucleosome arrays differ so much from natural chromatin.

An earlier study found that short nucleosome arrays with a yeast-like nucleosome-repeat length (167 bp) could form ordered, dispersed, 30-nm fibers *in vitro* (Routh et al., 2008). We did not observe such fibers. Instead, most yeast nucleosomes pack into a large mass without any regular motifs; in the few other cases, chromatin packs as irregular 30-nm fibers. The formation of chromatin masses can be explained by the interdigitation of fibers, i.e., inter-fiber interactions force the irregular 30-nm fibers to be in an unfolded state, mixed with the nucleosomes of other unfolded 30-nm fibers (Eltsov et al., 2008). These masses could also be explained by hierarchical loops, which are compatible with more heterogeneous packing than helical models (Grigoryev et al., 2016). More importantly, 30-nm fibers are found at the less-crowded periphery of chromatin mass *in vitro*. This phenomenon supports the idea that the chromatin crowding can prevent fiber formation. However, due to technical limitations, we cannot

exclude the possibility that the 30-nm fibers do not unfold, but are instead indistinguishable when closely packed (Grigoryev and Woodcock, 2012).

Chromatin is more compact *in vitro* than *in vivo*

Our cryo-ET studies of two organisms gives us a rare opportunity to assess the factors that contribute differences in 3-D chromatin organization *in vivo* and *in vitro*. One major difference is that nucleosomes pack slightly closer *in vitro* than *in vivo*, especially in yeast (Fig. 4 H and I). Although our lysis approach is gentle, it cannot keep chromatin remodelers and transcription factors from dissociating from the chromatin. The presence of such factors *in vivo* might prevent the chromatin from folding into a compact higher-order structure. This notion was supported by a study showing that when the Widom 601 nucleosome-positioning element was inserted into yeast genome, both the positioning and the occupancy changed substantially compared to *in vitro* chromatin arrays (Perales et al., 2011). We hypothesize that chromatin remodelers, transcription factors, and transcription itself keep chromatin dispersed *in vivo*; the absence of these factors *in vitro* allows chromatin segments to pack closer together.

MATERIALS AND METHODS

Picoplankton cell culture

Ostreococcus tauri cells (strain OTH95, Roscoff Culture Collection strain RCC 745) were grown in artificial seawater containing Sigma sea salt and Keller enrichment medium (Table S1) in a 12h:12h light:dark cycle. Lighting was provided by T5050 white light-emitting diodes, passed through a 'Moonlight blue' filter (Lee Filters, #183; Panavision, Los Angeles, CA). This setup produced an illuminance of ~ 400 - 500 lux when measured at the approximate position of the cells, with an Amprobe LM-100 digital light meter (Danaher, Inc., Everett, WA). Cells (30 - 50 ml) grown this way were loosely synchronized and were mostly in mid-G_1 phase at the beginning of the light phase (Corellou et al., 2005). The cells were harvested in mid-log phase (OD_{600} ~ 0.05 - 0.1) shortly after the light-to-dark transition and then pelleted by centrifugation at 5,000 × *g* for 10 minutes at 4°C.

Picoplankton lysis

Cells were then resuspended in 1 ml of prechilled (4°C) fresh artificial seawater and re-centrifuged at 5000 × *g* for 1 minute. The cell pellet was then resuspended in prechilled lysis buffer, yielding a final OD_{600} ~ 20. The cells were incubated on ice for either 7 - 9 minutes (1 mM Mg^{2+}) or 10 - 15 minutes (0 Mg^{2+} or 5 mM EDTA), measured from when the cells were resuspended in lysis buffer to the point of plunge freezing. Using a combination of sucrose and glycerol, the concentration of soluble particles (ions and undissociated molecules) in the lysis buffer was adjusted to ~820 mM, which is

383 approximately 4/5 of the concentration of soluble buffer molecules in artificial seawater
384 (~ 1 M); for details, see Table S2. The picoplankton burst in all lysis buffers. While the
385 plasma membrane was completely ruptured, the contents of the largest two organelles -
386 - the nucleus and the chloroplast -- remained physically associated. This association
387 was fortuitous because the chloroplast remnants, which were high contrast and could
388 be located even at low magnification, facilitated the search for the adjacent chromatin.
389
390 **Yeast nucleus isolation and lysis**
391 Nuclei were isolated using the Yeast nuclei isolation kit (Abcam 206997), with
392 modifications. Wild-type yeast (YEF473A; a gift from Kerry Bloom) cells were grown in
393 30 ml yeast peptone dextrose (YPD) medium to mid-log phase (OD_{600} ~ 1) in a shaker
394 (30°C, 250 RPM). The cells were pelleted by centrifuging at 3,000 × *g* for 5 minutes at
395 room temperature in 50 ml conical tubes, washed twice by resuspension in 1 ml H_2O,
396 then re-centrifuged at 3000 × *g* for 1 min. The cell pellet was then resuspended in 1 ml
397 Buffer A (containing 10 mM DTT, from the kit), and then incubated for 10 minutes in a
398 30°C water bath. Cells were then centrifuged at 1500 × *g* for 5 minutes and then
399 resuspended in 1 ml Buffer B (from the kit) containing lysis enzyme cocktail (diluted
400 1:1,000). The mixture was incubated in a 30°C shaker for 15 min, and then centrifuged
401 at 1,500 × *g* for 5 minutes at 4°C. The pellet was resuspended in 1 ml prechilled Buffer
402 C (from the kit) with protease inhibitor cocktail. The suspension was transferred to a
403 glass Dounce homogenizer on ice and then the cells were lysed with 15 strokes. The
404 suspension was incubated with shaking for 30 minutes at room temperature and was
405 then centrifuged at 500 × *g* for 5 minutes at 4°C to remove the debris. A small aliquot of

406 the supernatant was stained with 4′,6-Diamidino-2-phenylindole dihydrochloride (DAPI)
407 to verify that the isolated nuclei were abundant. The supernatant was then re-
408 centrifuged at 20,000 × *g* for 10 minutes at 4°C. The nuclear pellet was resuspended in
409 pre-chilled lysis buffer (see Table S2) and incubated for 15 minutes on ice prior to
410 plunge freezing.
411
412 **TSA treatment**
413 Wild-type yeast were grown in 30 ml YPD to mid-log phase (OD_{600} ~ 1) in a
414 shaker (30°C, 250 RPM). Cells were pelleted at 3,000 × *g* for 5 minutes and then
415 resuspended in 30 ml YPD with 16.4 μM TSA (5 mM stock in dimethyl sulfoxide, Sigma
416 T1952). The cells were then incubated for 1 hour at 30°C before nuclei isolation. During
417 nuclei isolation, the solutions used up to the spheroplasting step did not contain TSA.
418 After spheroplasting, all solutions contained 82 μM TSA.
419
420 **Plunge-freezing**
421 Colloidal gold (used for fiducial-based tomographic image alignment; see below)
422 has a tendency to aggregate in the presence of seawater unless first treated with bovine
423 serum albumin (BSA) (Gan et al., 2011). Therefore, the colloidal gold (20 nm, BBI
424 solutions, Cardiff, UK) was first suspended in 10 mg/ml BSA, pelleted at 18,000 × *g* for
425 5 minutes, and then the supernatant was discarded. The gold was treated with BSA
426 twice in this way. The BSA-treated gold was then added to the cells just before plunge-
427 freezing.

Grids (CF-4/2-2C-T and CF-2/2-2C-T, Protochips, Morrisville, NC) were plasma cleaned 90 seconds at 15 mA with a Emitech K100X glow-discharge unit. Treated cells (3 µl) were added to each side of a plasma-cleaned grid. The grids were blotted with filter paper (Whatman, Grade 1) for 1 second, blot force 1, followed by a 5-second wait time, then plunged into 67/33 (% v/v) liquid propane/ethane mixture (Tivol et al., 2008) using a Vitrobot, Mark IV (Thermo, Waltham, MA). The relative humidity in the sample chamber of the Vitrobot was kept at 100%. The grids were then stored in liquid nitrogen.

Cryo-ET and image processing

Data-collection parameters are detailed in Table S3. Tilt-series alignment and tomographic reconstruction were done using Etomo (Mastronarde, 1997). Because only the positions corresponding to the nuclear contents were of interest and because some sample positions warped during data collection, most tilt-series were aligned using only the gold fiducials in the vicinity of the nuclear densities. Some of the beads were automatically removed with the Etomo “bead eraser” tool. For yeast samples, all tilt series were aligned using patch tracking because of insufficient gold fiducial numbers. For yeast and picoplankton samples treated with 0 mM Mg^{2+} or with EDTA, the tilt series were first corrected for the effects of the contrast-transfer function and then 2-D low-pass filtered with cutoff in the range of 0.2 - 0.35 $pixel^{-1}$ and sigma value of 0.05 $pixel^{-1}$; these settings gently attenuated spatial-frequency components starting at 4.5-nm (picoplankton) to 2.6-nm (yeast) resolution. For picoplankton samples treated with 1 mM Mg^{2+}, the contrast was much lower due to sample thickness and crowding effects,

450 necessitating the two-fold binning of the tilt series to improve the visualization. Other
451 parameters were kept as Etomo defaults.
452
453 **Naked-DNA length analysis**
454 To facilitate the measurement of naked DNA length, the tomograms were binned
455 by 2 and then low-pass filtered (cutoff=0.3, sigma=0.05). DNA in a tomogram was
456 tracked semi-automatically using the Livewire drawing tool in 3dmod, saved as a model
457 file, then extracted with the IMOD program imodinfo.
458
459 **Template matching**
460 Template matching was done using PEET (Heumann, 2016). Two types of
461 templates were used for picoplankton: a featureless cylinder (6-nm thick, 10-nm
462 diameter), generated using beditimg (Heymann and Belnap, 2007); for yeast: a
463 subtomogram of a high contrast nucleosome-like particle was selected. The choice of
464 reference did not influence the subsequent analysis of most particles because a low
465 cross-correlation (CC) cutoff was used (see below) and the rotational alignment solution
466 was discarded prior to further analysis. For *O. tauri*, however, we found that hits
467 corresponding to nucleosomes with the superhelical axis nearly perpendicular to the ice
468 surface were off-center. These nucleosomes were better centered when we used a low-
469 pass-filtered subtomogram average of a RELION 3-D class as a reference (see below).
470 To minimize the effects of neighboring densities, subvolumes were isolated with a thick
471 cylindrical mask with a soft edge. To minimize the number of false negatives, we kept
472 the template-matching hits that were spaced as close as 6 nm, corresponding to face-

473 to-face packed nucleosomes. This minimum distance resulted in many “overlapped”
474 candidate nucleosomes (hits), of which one was removed automatically at each position
475 at the end of the search. To further minimize the number of false negatives, all hits with
476 a CC (relative to the template) greater than 0.2 were saved and then visualized in the
477 original tomogram; the CC values were displayed using the 3dmod “fine grain” feature.
478 The CC cutoff was then manually increased in 0.05 increments until most spurious hits
479 (carbon support edge, ice contaminants, and aggregates) were eliminated. The final
480 filtered hit list was then subject to heterogeneity analysis using RELION (see below).
481
482 **Nearest-neighbor distance analysis**
483 For a fair comparison between different datasets, we used the average of CC
484 coefficients of all template-matching hits as cutoff. For example, if the average CC value
485 in dataset A was 0.4 and the one in dataset B was 0.3, then we used 0.4 as cutoff for A
486 and 0.3 for B. We then made small adjustments to the CC cutoff to ensure the low
487 occurrence of obvious false positives (like ribosomes and ice) and false negatives. The
488 coordinates of the nucleosome hits were then imported into Matlab. NND and 10^{th} NND
489 were calculated using the Matlab function nearestneighbour.m. The script is available
490 upon request.
491
492 **Heterogeneity analysis and subtomogram averaging**
493 Subtomograms were analyzed using the subtomogram-averaging and classification
494 routines (Bharat et al., 2015; Bharat and Scheres, 2016) as implemented in RELION 1.4
495 and 2.0 (Kimanius et al., 2016; Scheres, 2012a, b). Because CTF phase flipping was

already done in IMOD, we disabled phase flipping in RELION. We also disabled the dose-weightage scheme because the images in the second half of the tilt series were severely underweighted due to the large cumulative dose. The missing-wedge effects were compensated for by the RELION CTF model. Candidate nucleosome positions were imported into RELION. Owing to the crowdedness of yeast nucleosomes, we used a smaller box (24 nm) and a smaller mask (17-nm diameter) for classification to exclude most densities of adjacent nucleosomes. Each nucleosome was averaged along the tomographic Z axis to produce a pseudo projection. These projections were then subjected to 2-D classification (50 or 100 classes). “Junk particles” such as ice, contaminants, or carbon-support features were manually removed. If the identity of the class ("junk” vs. real nucleosome) was ambiguous, the member particle positions were visualized in the context of the original tomogram, allowing for discrimination of junk and real particles. Our decisions to exclude/include ambiguous classes were guided by biologically meaningful features such as the size and shape of the density and the proximity to the other nucleosomes (chromatin-associated nucleosomes are not found “floating” alone). The remaining good particles were subjected additional rounds of 2-D classification and elimination of junk classes until only reasonable nucleosome-like classes remained.

To better discriminate between nucleosome conformational states, we performed 3-D classification without the use of an external reference. New junk classes were found and removed at the end of each round of classification. We found that the number of classes decreased as we increased the resolution used for classification to the Nyquist limit. This resolution dependency is probably due to the lower signal-to-noise ratio of the

519 higher-resolution data. Starting with 20 classes and using data to the Nyquist limit (20 Å
520 for yeast), fewer than 10 distinctive conformational classes remained at the end of 2 - 3
521 sequential classification-and-junk-removal rounds. These classes were then subjected
522 to synthetic tomogram construction. For picoplankton chromatin in 1 mM and 0 mM
523 Mg^{2+}, we also attempted 3-D classification of higher-order structures by increasing the
524 mask size, but found that most of the classes did not converge to anything biologically
525 meaningful, probably due to the extreme heterogeneity at the level of oligo-nucleosome
526 structures. Our 2-D classification of picoplankton chromatin in 5 mM EDTA failed to find
527 any convincing face-to-face or other abundant higher-order motifs because most of the
528 nucleosomes were too far apart to interact.
529
530 **Synthetic tomogram construction**
531 Template-matching hits that were subjected to the 2-D and 3-D classification
532 process were mapped back into a phantom volume the size of the original tomogram
533 using the EMAN2 program e2proc3d (Tang et al., 2007). The script to do this is
534 available upon request.
535
536 **Figures**
537 Density maps were rendered with UCSF Chimera (Pettersen et al., 2004).
538
539 **Data sharing**
540 Tilt series data of all samples presented in this paper have been made
541 accessible in the EMPIAR online database: (EMPIAR-10098). One example tomogram

each of picoplankton and yeast has been deposited in the EMDB (EMD-6737).

Acknowledgements

We thank the CBIS microscopy staff for support and training. We thank François-Yves Bouget for advice of Ostreococcus cell-culture conditions, Rado Danev for suggesting 2-D classification of subtomograms, and Kerry Bloom for yeast strains. We also thank the Gan team and David Shore for discussions. SC, YS, CC, and LG were supported by NUS startups R-154-000-515-133, R-154-000-524-651, and D-E12-303-154-217, a MOE T2 R-154-000-624-112, and a NUS YIA R-154-000-558-133.

Contributions

SC - experiments, project design, writing; YS - experiments; CC - experiments, editing; JS - training; LG - experiments, project design, writing.

555 **REFERENCES**

556

557 Athey, B.D., Smith, M.F., Rankert, D.A., Williams, S.P., and Langmore, J.P. (1990). The
558 diameters of frozen-hydrated chromatin fibers increase with DNA linker length: evidence
559 in support of variable diameter models for chromatin. J Cell Biol *111*, 795-806.

560 Bednar, J., Garcia-Saez, I., Boopathi, R., Cutter, A.R., Papai, G., Reymer, A., Syed,
561 S.H., Lone, I.N., Tonchev, O., Crucifix, C.*, et al.* (2017). Structure and Dynamics of a
562 197 bp Nucleosome in Complex with Linker Histone H1. Molecular cell *66*, 384-397
563 e388.

564 Bednar, J., Horowitz, R.A., Grigoryev, S.A., Carruthers, L.M., Hansen, J.C., Koster, A.J.,
565 and Woodcock, C.L. (1998). Nucleosomes, linker DNA, and linker histone form a unique
566 structural motif that directs the higher-order folding and compaction of chromatin. Proc
567 Natl Acad Sci U S A *95*, 14173-14178.

568 Bernstein, B.E., Tong, J.K., and Schreiber, S.L. (2000). Genomewide studies of histone
569 deacetylase function in yeast. Proc Natl Acad Sci U S A *97*, 13708-13713.

570 Bharat, T.A., Russo, C.J., Lowe, J., Passmore, L.A., and Scheres, S.H. (2015).
571 Advances in Single-Particle Electron Cryomicroscopy Structure Determination applied
572 to Sub-tomogram Averaging. Structure *23*, 1743-1753.

573 Bharat, T.A., and Scheres, S.H. (2016). Resolving macromolecular structures from
574 electron cryo-tomography data using subtomogram averaging in RELION. Nat Protoc
575 *11*, 2054-2065.

576 Brandt, F., Etchells, S.A., Ortiz, J.O., Elcock, A.H., Hartl, F.U., and Baumeister, W.
577 (2009). The native 3D organization of bacterial polysomes. Cell *136*, 261-271.

578 Chao, F.C. (1957). Dissociation of macromolecular ribonucleoprotein of yeast. Archives
579 of biochemistry and biophysics *70*, 426-431.

580 Chen, C., Lim, H.H., Shi, J., Tamura, S., Maeshima, K., Surana, U., and Gan, L. (2016).
581 Budding yeast chromatin is dispersed in a crowded nucleoplasm in vivo. Mol Biol Cell
582 *27*, 3357-3368.

583 Collins, N., Poot, R.A., Kukimoto, I., Garcia-Jimenez, C., Dellaire, G., and Varga-Weisz,
584 P.D. (2002). An ACF1-ISWI chromatin-remodeling complex is required for DNA
585 replication through heterochromatin. Nat Genet *32*, 627-632.

586 Corellou, F., Camasses, A., Ligat, L., Peaucellier, G., and Bouget, F.Y. (2005). Atypical
587 regulation of a green lineage-specific B-type cyclin-dependent kinase. Plant physiology
588 *138*, 1627-1636.

589 Dorigo, B., Schalch, T., Bystricky, K., and Richmond, T.J. (2003). Chromatin fiber
590 folding: requirement for the histone H4 N-terminal tail. Journal of molecular biology *327*,
591 85-96.

592 Dorigo, B., Schalch, T., Kulangara, A., Duda, S., Schroeder, R.R., and Richmond, T.J.
593 (2004). Nucleosome arrays reveal the two-start organization of the chromatin fiber.
594 Science *306*, 1571-1573.

595 Downs, J.A., Kosmidou, E., Morgan, A., and Jackson, S.P. (2003). Suppression of
596 homologous recombination by the Saccharomyces cerevisiae linker histone. Molecular
597 cell *11*, 1685-1692.

598 Eltsov, M., MacLellan, K.M., Maeshima, K., Frangakis, A.S., and Dubochet, J. (2008).
599 Analysis of cryo-electron microscopy images does not support the existence of 30-nm
600 chromatin fibers in mitotic chromosomes in situ. Proceedings of the National Academy
601 of Sciences *105*, 19732-19737.

602 Eltsov, M., Sosnovski, S., Olins, A.L., and Olins, D.E. (2014). ELCS in ice: cryo-electron
603 microscopy of nuclear envelope-limited chromatin sheets. Chromosoma *123*, 303-312.

604 Fei, J., Torigoe, S.E., Brown, C.R., Khuong, M.T., Kassavetis, G.A., Boeger, H., and
605 Kadonaga, J.T. (2015). The prenucleosome, a stable conformational isomer of the
606 nucleosome. Genes Dev *29*, 2563-2575.

607 Finch, J.T., and Klug, A. (1976). Solenoidal model for superstructure in chromatin.
608 Proceedings of the National Academy of Sciences *73*, 1897-1901.

609 Funke, J.J., Ketterer, P., Lieleg, C., Korber, P., and Dietz, H. (2016). Exploring
610 Nucleosome Unwrapping Using DNA Origami. Nano Lett *16*, 7891-7898.

611 Gan, L., Ladinsky, M.S., and Jensen, G.J. (2011). Organization of the smallest
612 eukaryotic spindle. Current biology : CB *21*, 1578-1583.

613 Gan, L., Ladinsky, M.S., and Jensen, G.J. (2013). Chromatin in a marine picoeukaryote
614 is a disordered assemblage of nucleosomes. Chromosoma *122*, 377-386.

615 Geiss, C.P., Keramisanou, D., Sekulic, N., Scheffer, M.P., Black, B.E., and Frangakis,
616 A.S. (2014). CENP-A arrays are more condensed than canonical arrays at low ionic
617 strength. Biophysical journal *106*, 875-882.

618 Grigoryev, S.A., Arya, G., Correll, S., Woodcock, C.L., and Schlick, T. (2009). Evidence
619 for heteromorphic chromatin fibers from analysis of nucleosome interactions. Proc Natl
620 Acad Sci U S A *106*, 13317-13322.

621 Grigoryev, S.A., Bascom, G., Buckwalter, J.M., Schubert, M.B., Woodcock, C.L., and
622 Schlick, T. (2016). Hierarchical looping of zigzag nucleosome chains in metaphase
623 chromosomes. Proc Natl Acad Sci U S A *113*, 1238-1243.

624 Grigoryev, S.A., and Woodcock, C.L. (2012). Chromatin organization - the 30 nm fiber.
625 Exp Cell Res *318*, 1448-1455.

626 Hansen, J.C. (2002). Conformational dynamics of the chromatin fiber in solution:
627 determinants, mechanisms, and functions. Annual review of biophysics and
628 biomolecular structure *31*, 361-392.

629 Hansen, J.C. (2012). Human mitotic chromosome structure: what happened to the 30-
630 nm fibre? The EMBO journal *31*, 1621-1623.

631 Heumann, J.M. (2016). PEET (University of Colorado Boulder).

632 Heymann, J.B., and Belnap, D.M. (2007). Bsoft: image processing and molecular
633 modeling for electron microscopy. Journal of structural biology *157*, 3-18.

634 Huff, J.T., and Zilberman, D. (2014). Dnmt1-independent CG methylation contributes to
635 nucleosome positioning in diverse eukaryotes. Cell *156*, 1286-1297.

636 Huynh, V.A., Robinson, P.J., and Rhodes, D. (2005). A method for the in vitro
637 reconstitution of a defined “30nm” chromatin fibre containing stoichiometric amounts of
638 the linker histone. Journal of molecular biology *345*, 957-968.

639 Jenuwein, T., and Allis, C.D. (2001). Translating the histone code. Science *293*, 1074-
640 1080.

641 Kimanius, D., Forsberg, B.O., Scheres, S.H., and Lindahl, E. (2016). Accelerated cryo-
642 EM structure determination with parallelisation using GPUs in RELION-2. Elife *5*.

643 Kubik, S., Bruzzone, M.J., Jacquet, P., Falcone, J.L., Rougemont, J., and Shore, D.
644 (2015). Nucleosome Stability Distinguishes Two Different Promoter Types at All Protein-
645 Coding Genes in Yeast. Molecular cell *60*, 422-434.

646 Lee, W., Tillo, D., Bray, N., Morse, R.H., Davis, R.W., Hughes, T.R., and Nislow, C.
647 (2007). A high-resolution atlas of nucleosome occupancy in yeast. Nat Genet *39*, 1235-
648 1244.

649 Lowary, P.T., and Widom, J. (1989). Higher-order structure of Saccharomyces
650 cerevisiae chromatin. Proc Natl Acad Sci U S A *86*, 8266-8270.

651 Luger, K., Mader, A.W., Richmond, R.K., Sargent, D.F., and Richmond, T.J. (1997a).
652 Crystal structure of the nucleosome core particle at 2.8 A resolution. Nature *389*, 251-
653 260.

654 Luger, K., Rechsteiner, T.J., Flaus, A.J., Waye, M.M., and Richmond, T.J. (1997b).
655 Characterization of nucleosome core particles containing histone proteins made in
656 bacteria. Journal of molecular biology *272*, 301-311.

657 Maeshima, K., Rogge, R., Tamura, S., Joti, Y., Hikima, T., Szerlong, H., Krause, C.,
658 Herman, J., Seidel, E., DeLuca, J.*, et al.* (2016). Nucleosomal arrays self-assemble into

659 supramolecular globular structures lacking 30-nm fibers. The EMBO journal *35*, 1115-
660 1132.

661 Mastronarde, D.N. (1997). Dual-axis tomography: an approach with alignment methods
662 that preserve resolution. Journal of structural biology *120*, 343-352.

663 Mavrich, T.N., Jiang, C., Ioshikhes, I.P., Li, X., Venters, B.J., Zanton, S.J., Tomsho,
664 L.P., Qi, J., Glaser, R.L., Schuster, S.C.*, et al.* (2008). Nucleosome organization in the
665 Drosophila genome. Nature *453*, 358-362.

666 McBryant, S.J., Adams, V.H., and Hansen, J.C. (2006). Chromatin architectural
667 proteins. Chromosome Res *14*, 39-51.

668 McDowall, A.W., Smith, J.M., and Dubochet, J. (1986). Cryo-electron microscopy of
669 vitrified chromosomes in situ. The EMBO journal *5*, 1395-1402.

670 Nathan, D., and Crothers, D.M. (2002). Bending and flexibility of methylated and
671 unmethylated EcoRI DNA. Journal of molecular biology *316*, 7-17.

672 Nishino, Y., Eltsov, M., Joti, Y., Ito, K., Takata, H., Takahashi, Y., Hihara, S., Frangakis,
673 A.S., Imamoto, N., Ishikawa, T.*, et al.* (2012). Human mitotic chromosomes consist
674 predominantly of irregularly folded nucleosome fibres without a 30-nm chromatin
675 structure. The EMBO journal *31*, 1644-1653.

676 Olins, A.L., and Olins, D.E. (1974). Spheroid chromatin units (v bodies). Science *183*,
677 330-332.

678 Perales, R., Zhang, L., and Bentley, D. (2011). Histone occupancy in vivo at the 601
679 nucleosome binding element is determined by transcriptional history. Mol Cell Biol *31*,
680 3485-3496.

681 Pettersen, E.F., Goddard, T.D., Huang, C.C., Couch, G.S., Greenblatt, D.M., Meng,
682 E.C., and Ferrin, T.E. (2004). UCSF Chimera--a visualization system for exploratory
683 research and analysis. Journal of computational chemistry *25*, 1605-1612.

684 Robinson, P.J., Fairall, L., Huynh, V.A., and Rhodes, D. (2006). EM measurements
685 define the dimensions of the “30-nm” chromatin fiber: evidence for a compact,
686 interdigitated structure. Proceedings of the National Academy of Sciences *103*, 6506-
687 6511.

688 Routh, A., Sandin, S., and Rhodes, D. (2008). Nucleosome repeat length and linker
689 histone stoichiometry determine chromatin fiber structure. Proc Natl Acad Sci U S A
690 *105*, 8872-8877.

691 Schalch, T., Duda, S., Sargent, D.F., and Richmond, T.J. (2005). X-ray structure of a
692 tetranucleosome and its implications for the chromatin fibre. Nature *436*, 138-141.

693 Scheffer, M.P., Eltsov, M., Bednar, J., and Frangakis, A.S. (2012). Nucleosomes
694 stacked with aligned dyad axes are found in native compact chromatin in vitro. Journal
695 of structural biology *178*, 207-214.

696 Scheffer, M.P., Eltsov, M., and Frangakis, A.S. (2011). Evidence for short-range helical
697 order in the 30-nm chromatin fibers of erythrocyte nuclei. Proceedings of the National
698 Academy of Sciences *108*, 16992-16997.

699 Scheres, S.H. (2012a). A Bayesian view on cryo-EM structure determination. Journal of
700 molecular biology *415*, 406-418.

701 Scheres, S.H. (2012b). RELION: implementation of a Bayesian approach to cryo-EM
702 structure determination. Journal of structural biology *180*, 519-530.

703 Shimamoto, Y., Tamura, S., Masumoto, H., and Maeshima, K. (2017). Nucleosome-
704 nucleosome interactions via histone tails and linker DNA regulate nuclear rigidity. Mol
705 Biol Cell.

706 Shivaswamy, S., Bhinge, A., Zhao, Y., Jones, S., Hirst, M., and Iyer, V.R. (2008).
707 Dynamic remodeling of individual nucleosomes across a eukaryotic genome in
708 response to transcriptional perturbation. PLoS Biol *6*, e65.

709 Song, F., Chen, P., Sun, D., Wang, M., Dong, L., Liang, D., Xu, R.-M., Zhu, P., and Li,
710 G. (2014). Cryo-EM study of the chromatin fiber reveals a double helix twisted by
711 tetranucleosomal units. Science *344*, 376-380.

712 Tang, G., Peng, L., Baldwin, P.R., Mann, D.S., Jiang, W., Rees, I., and Ludtke, S.J.
713 (2007). EMAN2: an extensible image processing suite for electron microscopy. Journal
714 of structural biology *157*, 38-46.

715 Thoma, F., and Koller, T. (1977). Influence of histone H1 on chromatin structure. Cell
716 *12*, 101-107.

717 Thomas, J.O., and Furber, V. (1976). Yeast chromatin structure. FEBS Lett *66*, 274-
718 280.

719 Tivol, W.F., Briegel, A., and Jensen, G.J. (2008). An improved cryogen for plunge
720 freezing. Microscopy and microanalysis : the official journal of Microscopy Society of
721 America, Microbeam Analysis Society, Microscopical Society of Canada *14*, 375-379.

722 Tse, C., Sera, T., Wolffe, A.P., and Hansen, J.C. (1998). Disruption of higher-order
723 folding by core histone acetylation dramatically enhances transcription of nucleosomal
724 arrays by RNA polymerase III. Mol Cell Biol *18*, 4629-4638.

725 van Holde, K., and Zlatanova, J. (1995). Chromatin higher order structure: chasing a
726 mirage? The Journal of biological chemistry *270*, 8373-8376.

727 Waterborg, J.H. (2000). Steady-state levels of histone acetylation in Saccharomyces
728 cerevisiae. The Journal of biological chemistry *275*, 13007-13011.

729 Widom, J. (1986). Physicochemical studies of the folding of the 100 A nucleosome
730 filament into the 300 A filament. Cation dependence. Journal of molecular biology *190*,
731 411-424.

732 Woodcock, C.L. (1994). Chromatin fibers observed in situ in frozen hydrated sections.
733 Native fiber diameter is not correlated with nucleosome repeat length. The Journal of
734 Cell Biology *125*, 11-19.

735 Woodcock, C.L., Frado, L.L., and Rattner, J.B. (1984). The higher-order structure of
736 chromatin: evidence for a helical ribbon arrangement. J Cell Biol *99*, 42-52.

737 Yao, J., Lowary, P.T., and Widom, J. (1990). Direct detection of linker DNA bending in
738 defined-length oligomers of chromatin. Proc Natl Acad Sci U S A *87*, 7603-7607.

739 Yuan, G.C., Liu, Y.J., Dion, M.F., Slack, M.D., Wu, L.F., Altschuler, S.J., and Rando,
740 O.J. (2005). Genome-scale identification of nucleosome positions in S. cerevisiae.
741 Science *309*, 626-630.
742

743 **LIST OF FIGURES**

1A	Schematic of chromatin states
1B	Cartoon of cell lysis scheme
1C	Intact Ot
1D	Lysed Ot
2A	Ot lysed, 1 mM Mg^{2+}
2B	Ot lysed, 0 Mg^{2+}
2C	Ot lysed, 5 mM EDTA
2D-G	Enlarged, cropped nucleosomes, fibers, masses
3A	Sc 0mM EDTA
3B	Sc 50 mM EDTA
3C,D	Enlargements of A+B fibers, 4-fold
4A,B	Sc -/+TSA
4C,D	Enlargement of ncps in B, 4-fold
4E,F	Enlargement of naked DNA in B, 4-fold
4G	Beeswarm plot of naked DNA in B
4H,I	NND and 10th NND of ncps in A, B, and *in vivo*
5A,B	Sc face-to-face and zigzags
5C	Sc 2D classes
5D	Sc 30-nm fibers
5E	Beeswarm plots of nucleosomes/11nm and fiber diameters
6A	Gallery of ncp 3-D classes
6B	Ot 5 mM EDTA, slicer
6C	Ot synthetic tomogram
7A	Gallery of ncp 3-D classes
7B,C	Enlargements of D,E
7D	Sc 50 mM EDTA, slicer
7F	Sc synthetic tomogram
8	Cartoon of nucleosome packing

744

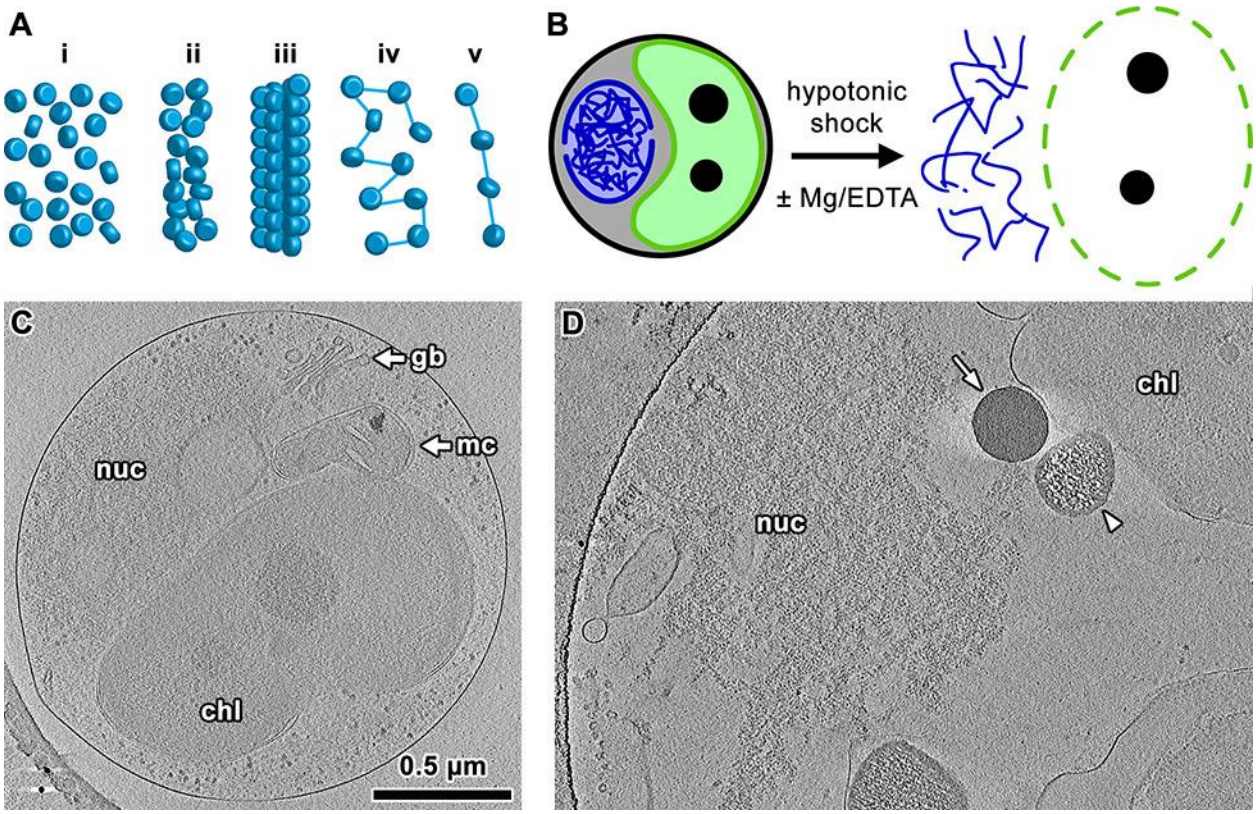

Figure 1. Strategy for 3-D analysis of natural chromatin

(A) Possible nucleosome (blue discs) arrangements, including (i) chromatin masses, (ii) irregular 30-nm fibers, (iii) regular 30-nm fibers, (iv) open zigzags, (v) beads on a string. Blue lines: linker DNA, depicted based on experimental observations. (B) The plasma membrane is ruptured by hypotonic shock, exposing the cellular contents to the final ionic conditions (with or without Mg^{2+} or EDTA added). The chloroplast (green) and nucleus (blue structure) are the two largest organelles in picoplankton. The dashed lines indicate the disruption of the plasma (black), chloroplast (green), and nuclear (blue) membranes. (C) Tomographic slice (30 nm) showing an intact early-interphase picoplankton cell. The largest organelles are labelled: chloroplast (chl); nucleus (nuc); Golgi body (gb); mitochondrion (mc). The lower left corner shows the curved edge of the carbon support and two gold fiducials (dark puncta). Note that as previously observed,

758 the nucleus is frequently found without an intact nuclear envelope even in interphase.
759 (D) Tomographic slice (30 nm) of a lysed picoplankton cell in 1 mM Mg^{2+}, at the same
760 scale as panel C. The arrow points to the radiation-tolerant granule from the chloroplast
761 and the arrowhead shows the chloroplast-derived granule that is sensitive to electron
762 beam damage. The remnants of the nucleus (nuc) and chloroplast (chl) are labelled.
763 The lysed cell is flattened by surface tension (after blotting), causing all components
764 components to spread out. This spreading allows the ice to be much thinner resulting in
765 higher image contrast than an intact cell.

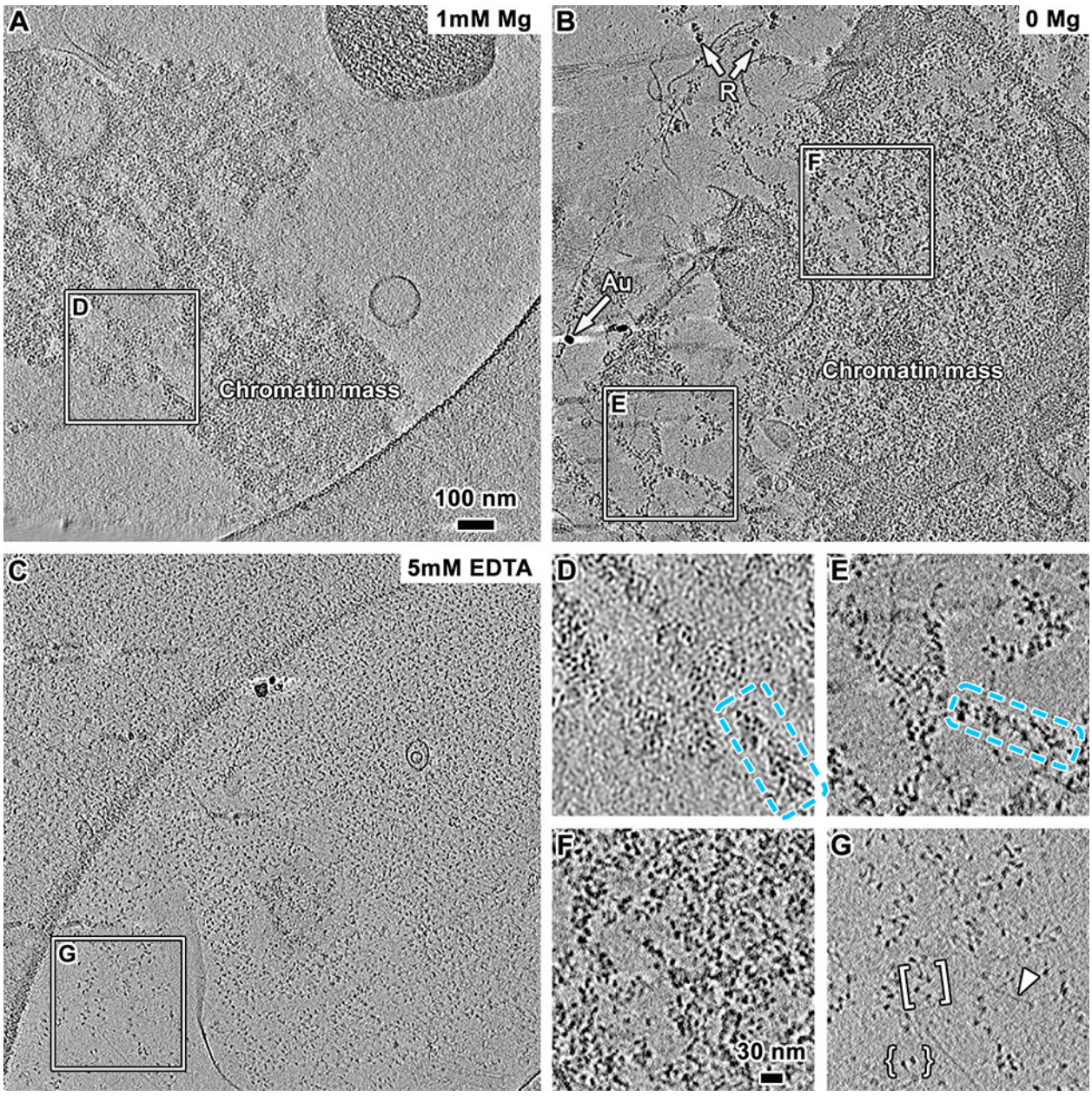

766

767 **Figure 2. Picoplankton chromatin can form masses and irregular 30-nm fibers in**

768 **the presence of divalent cations**

769 Tomographic slices (30 nm) of picoplankton cell lysates in buffer supplemented with (A)

770 1 mM Mg^{2+}, (B) no additional divalent cations, and (C) 5 mM EDTA. The dense round

771 structures are gold fiducials (Au in panel B); the gently curved structures in A and C are

772 from the edges of the carbon support film. A couple of ribosomes (R) are indicated with

773 arrows in (B). Positions boxed in A - C are enlarged 2-fold, showing irregular 30-nm
774 fibers (D-F), open zigzags (G, bracket), and a couple of nucleosomes (G, curly
775 brackets). A long stretch of naked DNA is indicated with an arrowhead in panel G. More
776 examples of chromatin subjected to each condition are shown in Figs S2 - S4.

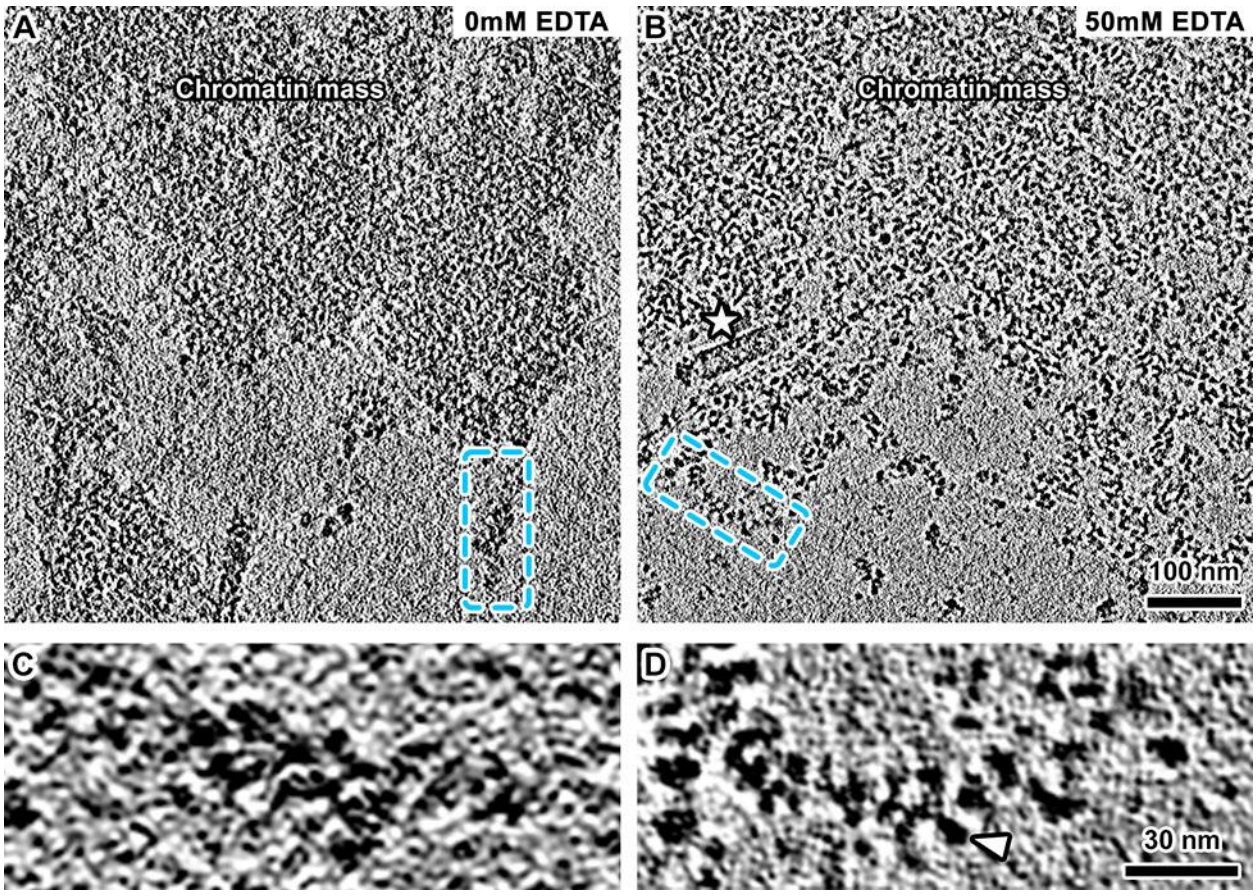

Fig. 3. Yeast chromatin forms masses and irregular 30-nm fibers even in the absence of divalent cations

(A) Tomographic slices (30 nm) of yeast nuclei lysate without EDTA. (B) Tomographic slices (30 nm) of yeast nuclei lysate with 50 mM EDTA. Star: microtubule. (C) Enlargement (4-fold) of 30-nm fiber boxed in panel A. (D) Enlargement (4-fold) of an irregular 30-nm fiber in 50 mM EDTA. Arrowhead: nucleosome.

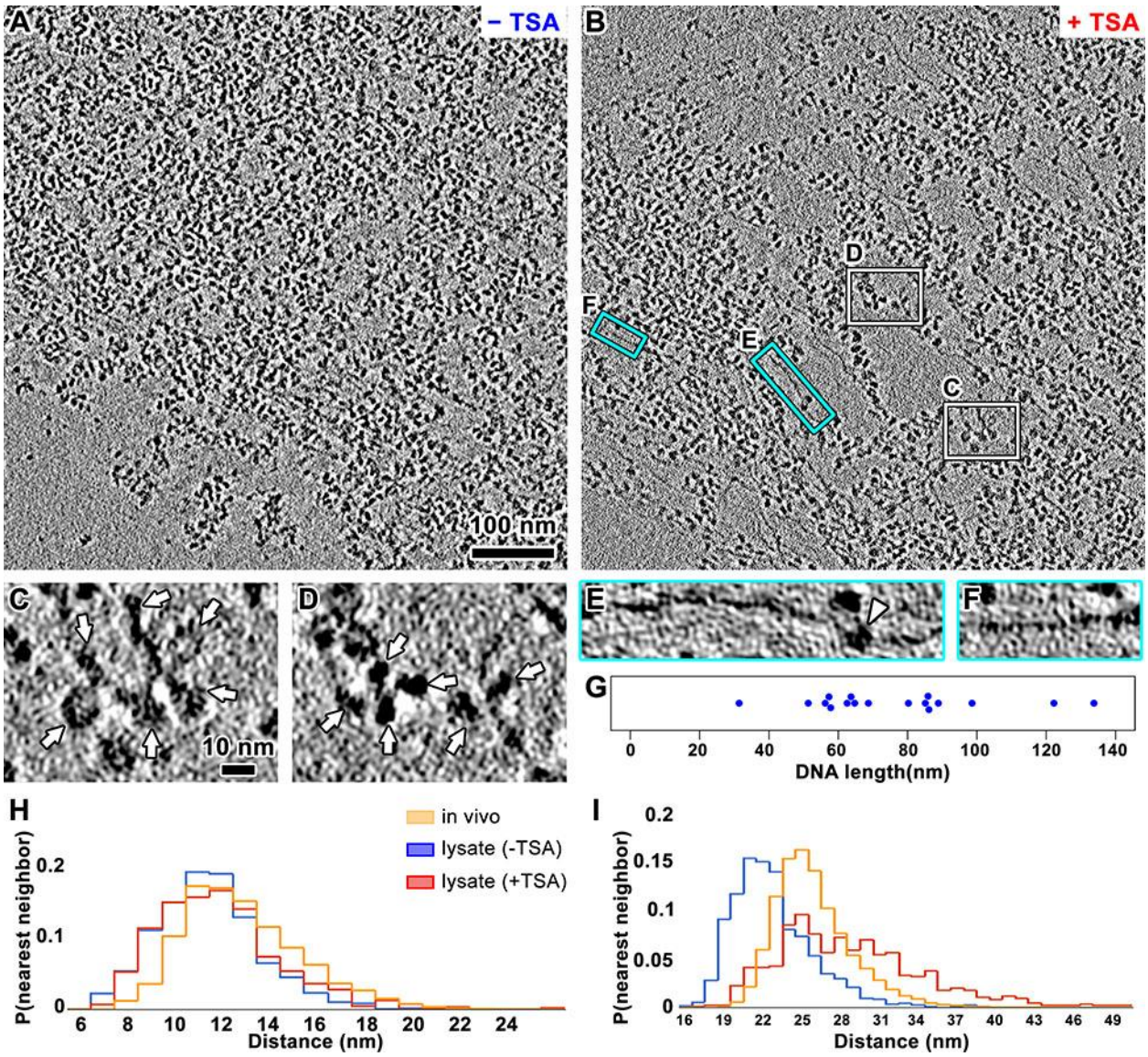

Figure 4. Inhibition of histone deacetylase partially disperses yeast chromatin

(A) Tomographic slice (10 nm) of yeast nuclei lysed in buffer with 50 mM EDTA. (B) Tomographic slice (10 nm) of yeast nuclei lysed in buffer with 50 mM EDTA and 82 μM TSA. (C and D) Four-fold enlargements of positions boxed in white in panel B, showing open zigzags. Arrows: nucleosomes. (E and F) Four-fold enlargements of positions boxed in cyan in panel B, rotated counter clockwise. The naked DNA is 110 nm long in panel E and 55 nm long in panel F. Arrowhead: a non-nucleosome density. (G)

792 Distribution of naked DNA length in tomograms of (B). (H and I) Histograms of nearest-
793 and tenth nearest-neighbor distances, respectively. The *in vivo* measurements were
794 done using a cryotomogram of sectioned yeast we previously reported (Chen et al.,
795 2016).

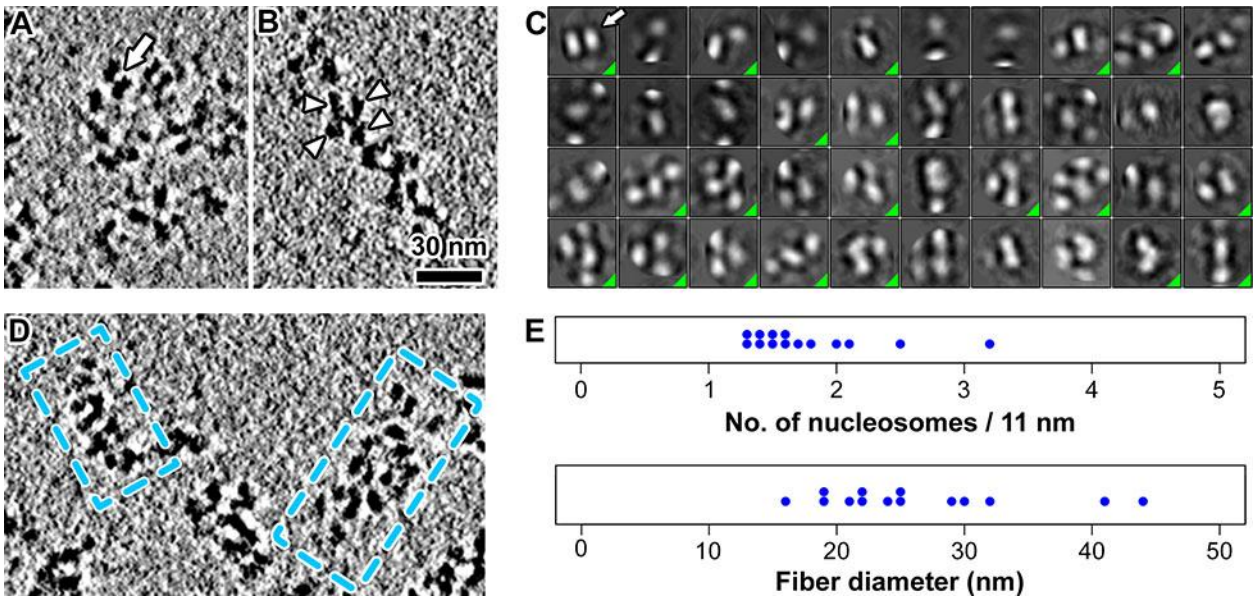

Figure 5. Natural chromatin adopts few regular packing motif

(A) Tomographic slice (10 nm) of yeast chromatin showing face-to-face packing (arrow). (B) Tomographic slice (6 nm) of yeast chromatin showing zigzag motif. Arrowheads: nucleosomes. (C) Two-dimensional classification of yeast lysate in 50 mM EDTA, ordered left-to-right, top-to-bottom from the most abundant to least abundant. Classes that represent actual nucleosome-nucleosome interactions have a green triangle in the lower-right corner. The contrast is inverted relative to the raw tomograms. Arrow: a class showing face-to-face packing. (D) Tomographic slice (10 nm) of yeast chromatin showing irregular 30-nm fibers. (E) Measurement of fiber compaction parameters.

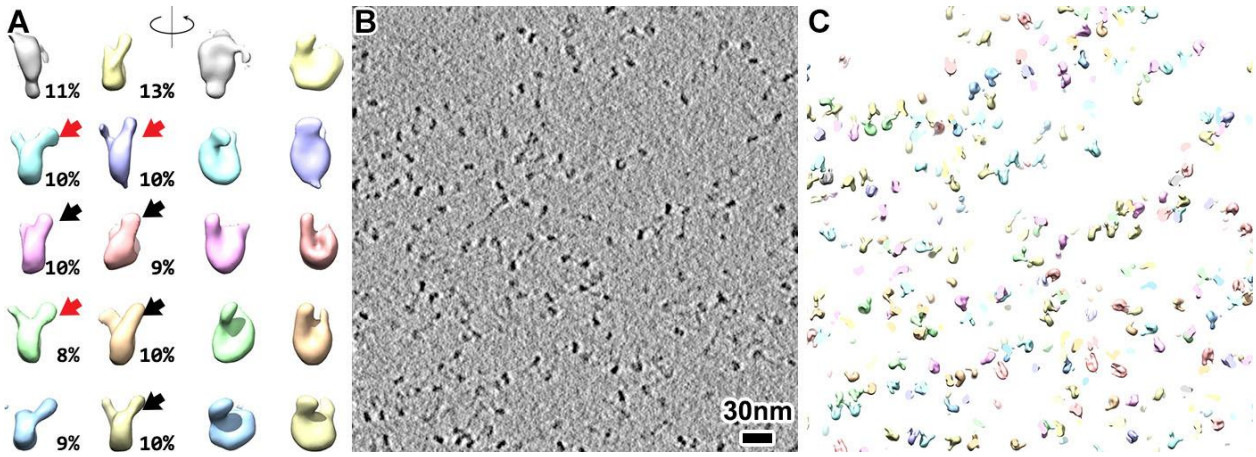

806

807 **Figure 6. Open zigzag chromatin accommodates open linker DNA**

808 Gallery of nucleosome classes viewed (left) edge on and (right) face on, contoured at
809 0.5σ to better visualize the linker DNA. The percentage of particles belonging is shown
810 in black numbers at the lower right of each respective class. Black arrows: classes with
811 open linker DNA. Red arrows: classes with crossed linker DNA. Notice that the yellow
812 and blue class only show the density of one linker DNA. (B) Tomographic slice (30 nm)
813 of picoplankton chromatin in lysis buffer with 5 mM EDTA. (C) Three-dimensional
814 classes of template-matched nucleosomes, remapped as a synthetic tomogram.

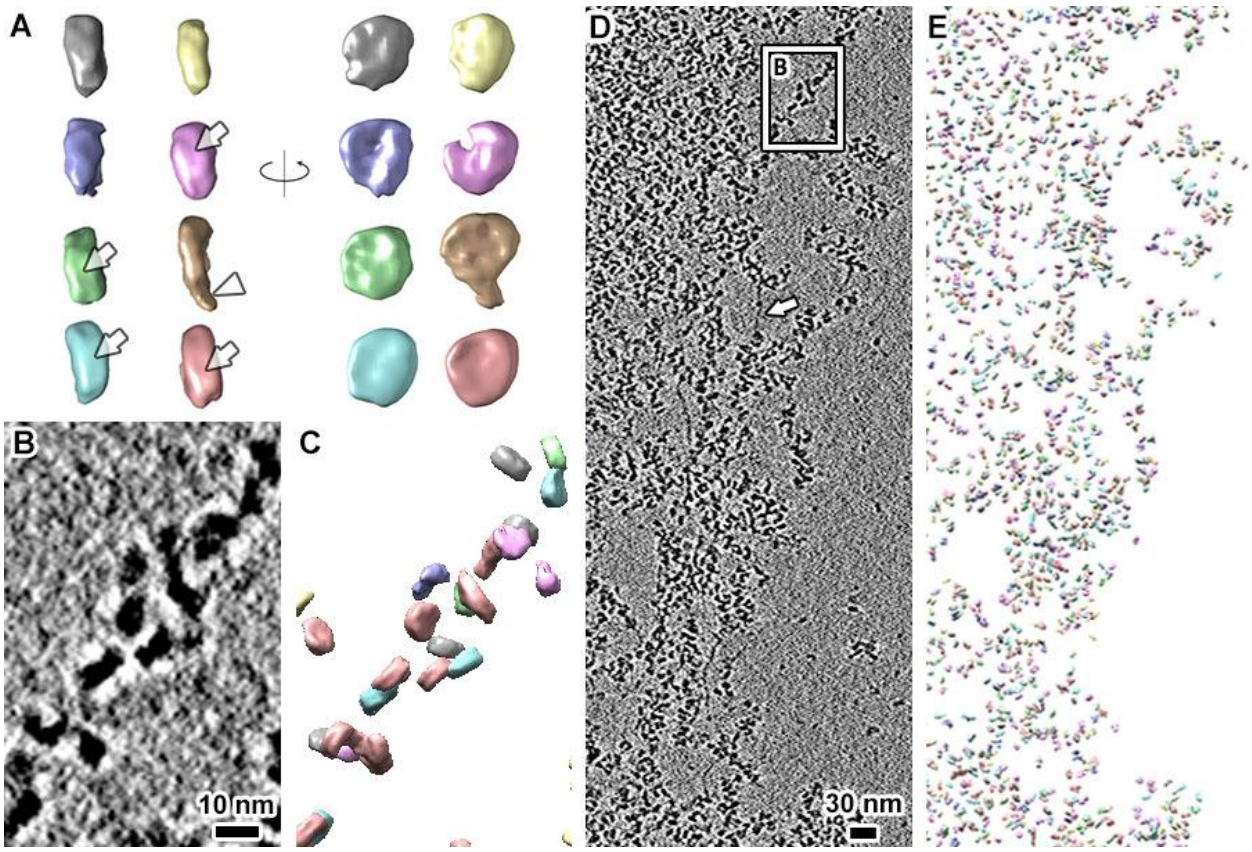

Figure 7. Synthetic tomogram reveals the conformational and configurational heterogeneity of yeast chromatin

(A) Gallery of 3-D classes viewed (left) edge on and (right) face on. Arrows: DNA gyres. Arrowhead: DNA stem-like structure. Note these nucleosome classes are not color coded the same way as in Fig. 4. (B) Five-fold enlargement of an irregular 30-nm fiber boxed in panel D. (C) synthetic tomogram of a 78-nm thick tomogram (same X-Y position as panel C). Arrow: a long stretch of naked DNA. (D) Tomographic slice (10 nm) of yeast nuclei lysed in the presence of 50 mM EDTA. (E) Synthetic tomogram of the same position as panel D).

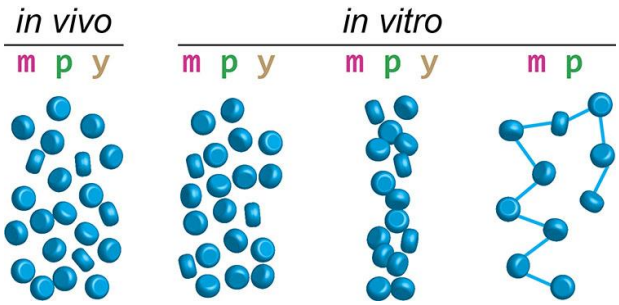

Figure 8. Chromatin structure is highly variable *in vitro*

Nucleosome (blue disc) packing in (m) metazoans, (p) picoplankton, and (y) yeast. *In vivo*, cryo-ET data is most consistent with a chromatin mass. *In vitro,* (left) masses, (middle) irregular 30-nm fibers, and (right) open zigzags have been seen in all three classes of organisms but very rarely in yeast. Linker DNA (blue lines) is depicted only in structures in which it has been observed.